Representation of Blowing Snow and Associated Visibility Reduction in an Operational High-Resolution Weather Model

Timothy D. Corrie III[a], Bart Geerts[a], Tatiana G. Smirnova[b,c], Stanley G. Benjamin[b,c], Michael Charnick[d], Matthew Brothers[d], Siwei He[e], Zachary J. Lebo[f], and Eric P. James[c]

[a] University of Wyoming, Laramie, WY

[b] Cooperative Institute for Research in Environmental Sciences (CIRES), University of Colorado, Boulder, CO

[c] NOAA Global System Laboratory, Boulder, CO

[d] National Weather Service, Cheyenne, WY

[e] Montana State University, Bozeman MT

[f] University of Oklahoma, Norman OK

Submitted to *Weather and Forecasting*

12 Nov 2023 – original submission

23 March 2024, 11 June 2024 – revised submissions

Corresponding author: Bart Geerts, Dept. of Atmospheric Science, University of Wyoming, Laramie WY 82071. Email: geerts@uwyo.edu

Early Online Release: This preliminary version has been accepted for publication in *Weather and Forecasting*, may be fully cited, and has been assigned DOI 10.1175/WAF-D-23-0195.1. The final typeset copyedited article will replace the EOR at the above DOI when it is published.

ABSTRACT

Blowing snow is a hazard for motorists because it may rapidly reduce visibility. Numerical weather prediction models in the United States do not capture the movement of snow once it reaches the ground, but visibility reductions due to blowing snow can be diagnosed based on model-predicted land surface and environmental conditions that correlate with blowing snow occurrence. A recently developed diagnostic framework for forecasting blowing snow concentration and the associated visibility reduction is applied to High-Resolution Rapid Refresh (HRRR) and Rapid Refresh Forecast System (RRFS) model output including surface snow conditions to predict surface visibility reduction due to blowing snow. Twelve blowing snow events around Wyoming from 2018 to 2023 are examined. The analysis shows that visibility reductions due to blowing snow tend to be overpredicted, caused by the initial assumption of full *driftability* of the snowpack. This study refines the aging of the blowing snow reservoir with two methods. The first method estimates driftability based on time-varying snow density from the RUC Land-Surface Model (RUC LSM) used in the HRRR and experimental RRFS models and is evaluated in a real-time context with the RRFS model. The second, complementary method diagnoses snowpack driftability using a process-based approach that requires data for recent snowfall, wind speed, and skin temperature. Compared to the full driftability assumption, this method shows limited improvements in forecasting skill. In order to improve model-based diagnosis of visibility reduction due to blowing snow, empirical work is needed to determine the relation between snowpack driftability and the recent history of snowfall and other weather conditions.

SIGNIFICANCE STATEMENT

Blowing snow presents a significant hazard to motorists and airport operations through sometimes very rapid and intense reductions in visibility, yet little predictive guidance exists for blowing snow. This study aims to improve the prediction of blowing snow occurrence and associated surface visibility reduction using diagnostics from an operational high-resolution weather model. One key challenge regards the question of *driftability* of the snowpack. This study evaluates two approaches to quantify driftability in terms of visibility reduction due to blowing snow and acknowledges that more measurements are needed to improve the

Accepted for publication in *Weather and Forecasting.* DOI 10.1175/WAF-D-23-0195.1.

representation of blowing snow physics in NWP models.

1. Introduction

Blowing snow (BLSN) presents a significant hazard to motorists because of the sometimes very rapid reductions in visibility associated with gusty winds lofting recently fallen snow into the air. A less hazardous but still potentially impactful phenomenon is drifting snow, where wind picks up snow, but the snow remains close to the ground. Drifting snow doesn't have the impact on visibility that BLSN does, but still impacts road surface conditions. Both hazards represent a challenge to autonomous driving technology. Within the United States, BLSN occurs most frequently in the northern Great Plains and northern Rockies, especially in south-central Wyoming (Fig. 1). Intense BLSN events (i.e. blizzards, events that cause visibility to decrease below ½ mi) are most impactful. Such events have led to numerous vehicle crashes, sometimes chain-reaction pile-ups (USDOT 2018) and may significantly disrupt life in large population centers such as Chicago, Minneapolis, Denver, as well as cities in the Canadian Prairie Provinces. The section of Interstate 80 across southern Wyoming, which is heavily used by the long-haul trucking industry (FHWA 2016), experiences ~17 road closures per year, averaging roughly 8 hours in duration, and most of them associated with BLSN (Saha et al. 2015). Some of these closures are in response to vehicle crashes, but increasingly they are imposed as a preventative measure. Reduced visibility from blowing snow can also hamper runway operations at airports.

Accepted for publication in *Weather and Forecasting.* DOI 10.1175/WAF-D-23-0195.1.

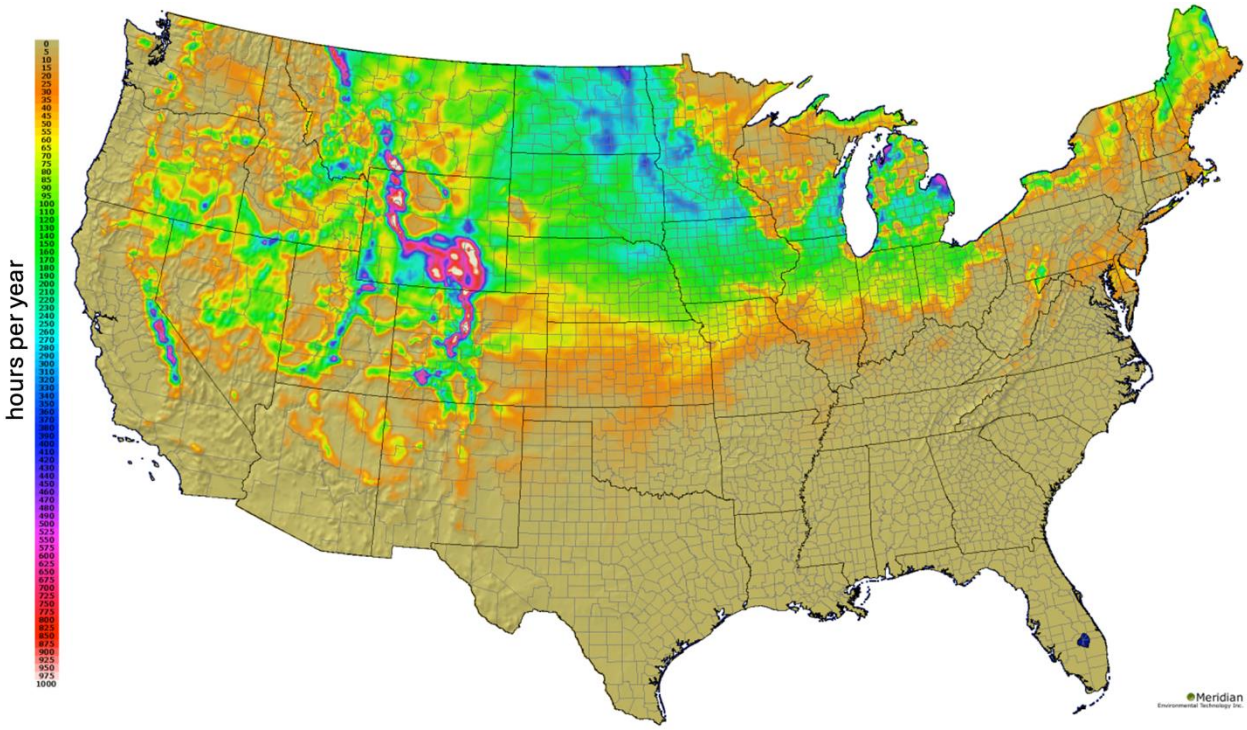

Fig. 1. Estimated frequency of BLSN (hours per year) across the United States, based on six years of North American Mesoscale (NAM) model data and snow cover data (source: Mewes 2012).

Freshly fallen dry snow is especially subject to wind-induced movement, through mechanisms like saltation (particles transported short distances at low heights) and suspension (particles lifted higher and transported further). The saltation layer typically is quite thin, a few cm deep. To a first order, BLSN saltation and suspension processes are analogous to driving dust and sand storms that erode soils and build dune landscapes (e.g., Greeley and Iverson 1985). But BLSN physics are more complex than sand particle physics, because of ice particle sublimation, accretion, fusion (either through melting or sintering) and splintering that may occur (e.g., He and Ohara 2017). Snow models that capture the full dynamics and thermodynamics of the snowpack have been built (e.g., Vionnet et al. 2013).

However, current-generation numerical weather prediction (NWP) models do not simulate the redistribution of snow after it has fallen on the ground, even though BLSN may affect surface weather conditions (in particular, visibility) and even fresh precipitation through the initiation of ice in shallow supercooled liquid clouds (e.g., Geerts et al. 2015). The prediction of BLSN by the United States National Weather Service (NWS) builds on empirical dependencies on weather (wind and temperature) and snowpack conditions. These empirical

Accepted for publication in *Weather and Forecasting*. DOI 10.1175/WAF-D-23-0195.1.

relations were originally developed based on data collected in the Canadian Prairie and Arctic regions (e.g., Pomeroy et al. 1993; Déry and Yau 1999), and have been used also in snow transport models. Initially a monodisperse BLSN particle size was assumed (Déry and Yau 1999) and later a two-moment BLSN particle size distribution (Déry and Yau 2001). Successive studies improved specific components of these BLSN models, such as sublimation physics (Déry and Yau 2002) (to account for the fact that under dry windy conditions sublimation of BLSN particles can significantly reduce the impact of BLSN on visibility reduction), and an improved threshold friction wind speed (He and Ohara 2017). These algorithms have been further refined and applied in the United States (e.g., Letcher et al. 2021) and elsewhere (e.g., Naaim-Bouvet et al. 2010).

Progress has been made in the measurement of BLSN particle concentration, size distributions, particle shape, and the vertical distribution of BLSN mass fluxes using a variety of instruments, including camera systems (Gordon and Taylor 2009), a Snow Particle Counter (Bellot et al. 2011), a Cloud Particle Imager (Lawson et al. 2006), and BLSN mass flux acoustic sensors (Chritin et al. 1999; Xie et al. 2023).

These tools, along with standard weather instruments to document ambient wind, gustiness, temperature, and radiative fluxes, have been used to predict BLSN probabilities based on ambient weather and surface snow conditions. One approach uses a *credibility parameter* (CRED), which attempts to assign a probability of a BLSN event given observations of the 10 m wind speed, 2 m air temperature, and the rough age of the snowpack or its upper layer (Baggaley and Hanesiak 2005; Vionnet et al. 2013). This method (with CRED probabilities ranging from 0 to 1) has been used by the NWS to forecast BLSN probability and intensity. Additionally, the Winter Storm Severity Index (WSSI) is utilized by NOAA to predict the impacts of winter weather factors including BLSN (Semmens et al. 2023). However, these impacts are assessed categorically, and in a rather ad hoc fashion, using wind speed and snowfall to estimate hourly visibilities at human eye level (~1.5 m) and calculate categories based on these visibilities (e.g. < 0.25 mi is in the moderate category). Currently, these algorithms are being fine-tuned and will include compatibility with 6-h National Digital Forecast Database (NDFD) data (D. Tobin, NOAA, 2024, personal communication). While WSSI can be a great forecasting tool, more in-depth measurements of the intensity, frequency, and particle properties of BLSN are needed to improve parameterizations of BLSN including visibility reduction.

Accepted for publication in *Weather and Forecasting.* DOI 10.1175/WAF-D-23-0195.1.

Progress has been made also with automated real-time BLSN alerting systems using Machine Learning techniques. For instance, McCorkle et al. (2021) used neural networks informed by roadside webcams to categorically identify BLSN events and characterize their intensity. Burrows and Mooney (2021) used a model-based Random Forest algorithm that combines METAR data and NWP models to determine what meteorological and environmental factors best predict severe BLSN (referred to as blizzard) events in Canada. Such alerting systems are expected to improve with denser sensor networks and more training data.

The main uncertainty in BLSN prediction regards *driftability* of the snow surface. Driftability refers to how easily snow can be picked up by the wind. It is dependent on the temperature and humidity of recently fallen snow, as well as skin (surface) temperature history (impacted by air wet-bulb temperature and net radiation) and snowpack age since the last snowfall (Purves et al. 1998). Driftability is impacted also by the recent history of snow drifting, as BLSN "reservoirs" can be depleted easily and the remaining snow becomes increasingly difficult to move. Variations in driftability must be considered to predict the probability and intensity of BLSN. In this paper, we estimate the snow driftability based on the recent history of model-resolved snowfall, temperature (air and skin), wind speed, and relative humidity. The relationships assumed in this study build on limited available empirical evidence.

While driftability is simple to conceptualize, it is difficult to accurately measure (e.g., Guyomarc'h et al. 1998; Vionnet et al. 2012). These two studies include a snow 'structure' parameter, a measure of snow/ice particle shape and intricacy. While this parameter is useful for snowpack models, the land surface scheme in NWP models does not predict such parameter, making it difficult for NWP models to estimate driftability this way. One alternative, tested in this paper, is to use a prognostic snow density, available in the Rapid Update Cycle (RUC) LSM (Smirnova et al. 2000, 2016). The RUC LSM is used in the NOAA High-Resolution Rapid Refresh (HRRR) model and in the NOAA Rapid Refresh Forecast System (RRFS) model currently planned for implementation in 2025.

This study has two objectives: One, it aims to predict BLSN occurrence and associated surface visibility reduction using diagnostics from an operational NWP model. Two, it lays out two frameworks for testing driftability: one incorporates time-dependent prognostic snow density (referred hereafter as the "operational" approach), and the other uses a history-based approach (referred hereafter as the "research" approach). The operational approach will focus on a single

Accepted for publication in *Weather and Forecasting.* DOI 10.1175/WAF-D-23-0195.1.

event in the Northern U.S. in the 2023-24 season, while the research approach focuses several cases in and around Wyoming, which is a hot spot for BLSN (Fig. 1). Section 2 describes how visibility reduction due to BLSN is calculated, what model diagnostics are used, and how the results are validated. Additionally, we step through both the operational (Section 2.c) and research (Section 2.d) approaches for estimating driftability. Results are described in Section 3. Section 4 discusses the implications and limitations of this study, and Section 5 lists the conclusions.

2. Data and methods

a. The High-Resolution Rapid Refresh (HRRR) Model

This study uses the NOAA operational HRRR weather model (Dowell et al. 2022; James et al. 2022, Benjamin et al. 2016) including the RUC LSM first incorporated into the operational NOAA RUC weather forecasting system (Benjamin et al. 2004). The RUC LSM has nine vertical levels in soil and a two-layer snow model (Smirnova et al. 2000, 2016). The RUC-LSM snow module accumulates snow on the ground using temperature-dependent variable density of frozen precipitation and solves the surface energy budget to compute snow melting and water refreezing. The RUC LSM produces predictions of snow water equivalent, snow depth, density of snowpack and snow temperature at all levels in snow. Snow variables are cycled in HRRR and once per day, snow cover gets updated using the 4-km resolution snow cover information from the NOAA Multisensor Snow and Ice Mapping System (IMS). The snow/land assimilation process is described in Benjamin et al. (2022). Visibility is diagnosed for the HRRR model as described in Benjamin et al (2021) including attenuation effects from cloud droplets and falling snow but not from blowing snow.

b. Calculating visibility reduction due to BLSN

The BLSN visibility reduction framework is adapted from Letcher et al. (2021) (hereafter referred to as L21). L21 uses a diagnostic framework connecting the saltation layer to the atmospheric surface layer above to estimate snow transport and visibility reduction using output from a Weather Research and Forecasting (WRF) model simulation for an intense BLSN event that impacted the north-central United States. The L21 WRF setup uses the Noah Multi-Parameterization (Noah MP) Land Surface Model (LSM) (Niu et al. 2011) and a sufficiently

Accepted for publication in *Weather and Forecasting.* DOI 10.1175/WAF-D-23-0195.1.

high inner-domain resolution to capture boundary layer circulations and fine-scale variations in land cover. L21 assumes the snow to be fresh, dry, and widespread, and as such perfectly *driftable*, conditions that undoubtedly applied to the freshly fallen snow case described in L21. They use the model output to compute the BLSN saltation rate, Q_s (kg m^{-1} s^{-1}), as in Pomeroy and Gray (1990):

$$Q_s = \frac{0.68}{u_*}\left(\frac{\rho_a}{g}\right) u_{*t}(u_*^2 - u_{*t}^2) \quad (1)$$

where u_* is the friction velocity (m s^{-1}) from HRRR model output, ρ_a is the air density (kg m^{-3}), g is the gravitational acceleration (9.81 m s^{-2}), and u_{*t} is the threshold friction velocity (m s^{-1}) for BLSN to occur. Here, we are treating u_{*t} as a constant (0.2 m s^{-1}), following L21, although this variable could be refined empirically as a function of the characteristics of the snow surface (He and Ohara 2017). The friction velocity and air density are calculated as part of the HRRR post-processing. Additionally, the height of the top of the saltation layer, z_r (m) is calculated from u_* (Liston and Sturm 1998) as:

$$z_r = 1.6\frac{u_*^2}{2g} \quad (2)$$

This equation is taken from empirical blowing sand models and adapted to BLSN. For typical friction velocity values over pasture and cropland, z_r is on the order of a few centimeters. From (2), the reference level (i.e. z_r) BLSN concentration, C_r (kg m^{-3}) (Vionnet et al. 2014) can be calculated as

$$C_r = \frac{Q_s}{u_p}\frac{\lambda g}{u_*^2}\exp\left(-\frac{\lambda z_r g}{u_*^2}\right) \quad (3)$$

where Q_s is calculated from Equation (1), z_r is calculated from Equation (2), λ is a dimensionless constant equal to 0.45, and u_p is the mean particle speed (m s^{-1}). We use $u_p = 2.8u_{*t}$, compared to $u_p = 1.6u_{*t}$ in L21, based on an unpublished analysis by Ted Letcher (2023, personal communication) and Equation 15 in Liston and Strum (1998). This error probably has a negligible effect on the overall visibility in the L21 study (T. Letcher, 2023, personal communication). We then calculate the average BLSN concentration at a height above ground level (AGL), $c(z)$, where z is the desired height AGL in meters:

$$c(z) = C_r \exp\{-1.55[(0.05628u_*)^{-0.544} - z^{-0.544}]\} \quad (4)$$

Accepted for publication in *Weather and Forecasting*. DOI 10.1175/WAF-D-23-0195.1.

where C_r is calculated from Equation (3). Note that this formulation has BLSN concentration decaying exponentially with height. BLSN concentration and surface visibility reduction are computed at a height of 2 m. This is common practice for BLSN (Pomeroy and Male 1992) and for other particles (e.g., dust and other aerosols).

The second part of the framework takes this BLSN concentration and computes a visibility (Pomeroy and Male 1998; Horvath 1971). The visibility calculation assumes that the BLSN particle size distribution is described by a gamma distribution. L21 use the following gamma-distribution shape-correction factor, c_α (dimensionless) following Pomeroy and Male (1988):

$$c_\alpha = \frac{(\alpha+1)!\alpha}{(\alpha+2)!} \tag{5}$$

Where α is the gamma-function shape parameter (dimensionless). This study assumes a value of $\alpha = 15$ (L21; Huang et al. 2008). The remaining two equations in the L21 framework (from Pomeroy and Male 1988),

$$\overline{Q_{ext}} = 1.82(\overline{r})^{-0.011} \text{ and } V = \frac{5.217\overline{r}\rho_p}{c(z)\cdot\overline{Q_{ext}}\cdot c_\alpha},$$

is combined to produce the visibility equation,

$$V = \frac{5.217\rho_p}{1.82c(z)c_\alpha}(\overline{r})^{1.011} \tag{6}$$

where $c(z)$ is calculated from Equation (4), c_α is calculated from Equation (5), $\overline{r}$ is the mean particle radius (m), and ρ_p is the snow density (kg m^{-3}). L21 assumed ρ_p to be 917 kg m^{-3}, which is the density of solid ice.

c. A snow-density-based driftability correction

Snowpack density can be used as a proxy for snow age, as older snow compacts and thus becomes less driftable. First, we estimated a variable, prognostic snowpack density, calculated as the ratio of snow water equivalent (SWE, expressed in kg m^{-2}) to snow depth ($SNOD$, m):

$$\rho_{p-modified} = \frac{SWE}{SNOD} \tag{7}$$

Both variables are available prognostic variables from the RUC LSM available for WRF and used in the HRRR, RAP, and RRFS models. Snow density (kg m^{-3}) is modified over time in the HRRR and RRFS models by compaction, melting, refreezing of water, and the addition of fresh

Accepted for publication in *Weather and Forecasting*. DOI 10.1175/WAF-D-23-0195.1.

snow (Smirnova et al. 2000). Examples of RRFS snow depth and snow density (within the snow cover) are shown in Fig. 2. Snow density from the RUC LSM can range from 58 kg m^{-3} (very fresh snow on bare soil) to ~500 kg m^{-3} (for older snow with some melting and compaction). The inverse of the snow density, multiplied by the density of liquid water, is the snow-liquid ratio (SLR), ranging in this case from over 10:1 (fresh snow) to ~2.5:1 (old snow) (Fig. 2b).

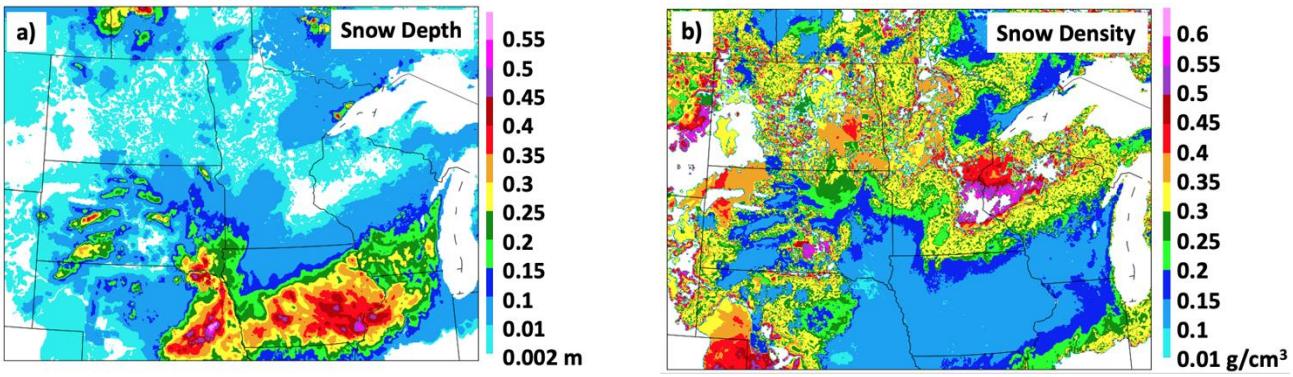

Fig. 2. (a) Snow depth (units m) and (b) snow density (g cm^{-3}) from the NOAA experimental RRFS weather model 3-h forecast for 12 January 2024 valid at 1800 UTC.

The mean radius $\overline{r}$ of BLSN particles has been shown to vary broadly (e.g. Liston and Sturm 1998, Huang et al. 2008, Yu et al. 2020). While L21 uses $\overline{r} = 30$ μm, we use a value $\overline{r}$ =200 μm, as discussed further in Section 2.e. The extinction coefficient (m^{-1}) for BLSN (Horvath 1971) is calculated as:

$$\beta = \frac{3.912}{V} \tag{8}$$

where V is the visibility (m) from Equation (6). The overall visibility reduction is based on the sum of all extinction coefficients: there are β values for the various water species including cloud water (i.e., fog) and snow, as well as dust and smoke. This sum then is used to compute overall visibility, i.e., the visibility is inversely proportional to the sum of extinction coefficients. The coefficient constants used for the HRRR and RAP models are listed in Benjamin et al. (2021), which are modified from those listed in Stoelinga and Warner (1999). We combine the β value corresponding to the original HRRR visibility with the BLSN β value (Equation (8)) and then calculate the combined visibility using the same Equation (8), rewritten to solve for V. Tests of the original formulation with Equation (8) result in an excessive reduction overall in visibility from BLSN, as shown in Fig. 3. This excessive BLSN effect on visibility reduction frequently was seen in experimental RRFS forecast for the month of March 2023.

Accepted for publication in *Weather and Forecasting*. DOI 10.1175/WAF-D-23-0195.1.

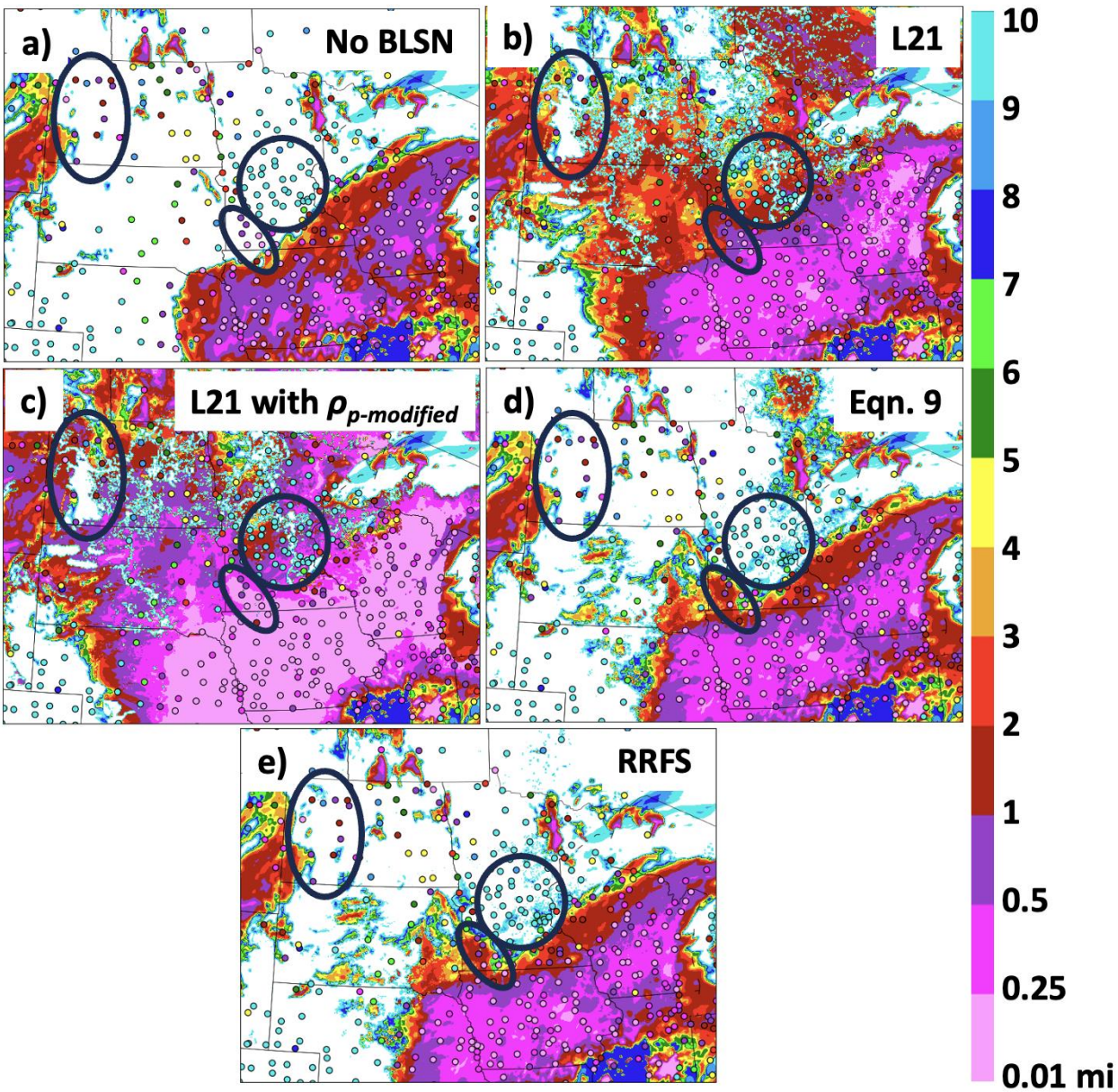

Fig. 3. Surface visibility (miles) with different diagnostics for case study from 12 January 2024. Surface visibility (miles) from experimental RRFS 3-h forecasts (valid 1800 UTC 12 January 2024, same case as in Fig. 2), showing a) without any BLSN component, b) L21, c) L21 with modified snow density using Eqn. (7), d) formulation using Eqn. (9), and e) current RRFS implementation in Eqn. (9) but also including roughness length restriction (see text). Observed visibilities at ASOS sites are overlaid as small circles using the same color bar. The black ovals indicate focus areas (one in western ND and two in southern MN) of how each specific framework modification affects visibility forecasts.

Accepted for publication in *Weather and Forecasting*. DOI 10.1175/WAF-D-23-0195.1.

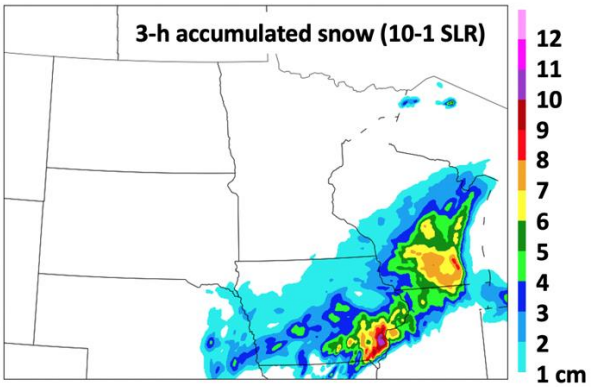

Fig. 4. 3-h accumulated snowfall (cm) from the experimental RRFS model for the 12 January 2024 case (same case shown in Fig. 3) predicted for 1500-1800 UTC.

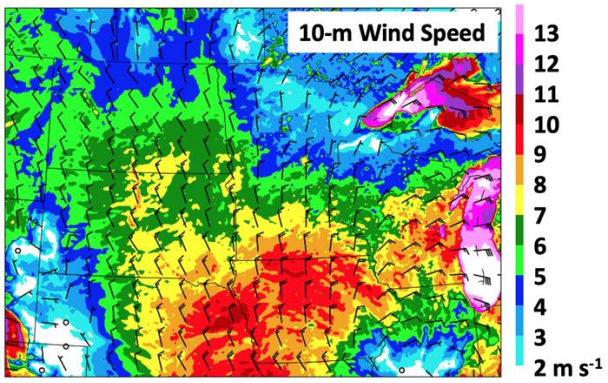

Fig. 5. 10-m wind speed (m s^{-1}) from the 3-h RRFS forecast valid at 1800 UTC 12 January 2024, the same case as shown in Figs. 3 and 4.

Therefore, to improve visibility forecasts, the visibility calculation (Equation 6) was modified as follows:

$$V = \frac{5.217\left(2\rho_{p-modified}+10max(0,\rho_{p-modified}-150)\right)}{1.82c(z)c_{\alpha}}(\overline{r})^{1.011} \quad (9)$$

This modification in Equation (9) using $\rho_{p-modified}$ allowed a visibility value for fresh snow about 25% larger than the L21 value which uses a fixed ρ_p value of 917 kg m^{-3}. But for older snow, Equation (9) gave much larger visibility and much less BLSN-related attenuation, as discussed earlier to represent the estimate driftability using the time-varying snow density in Equation (7). The inflation factor allowed reasonable BLSN visibility for fresh snow (SLR ~ 10:1) but as needed, produced much higher visibility (less BLSN attenuation) for older, denser snowpack.

Accepted for publication in *Weather and Forecasting*. DOI 10.1175/WAF-D-23-0195.1.

An intercomparison between different BLSN visibility options are shown in Fig. 3 for a RRFS forecast from 12 January 2024 for a case with substantial blowing snow reduction in visibility. Observed visibilities from ASOS (Automated Surface Observation System) sites are overlaid in each panel. The ovals in each panel highlight three regions of interest. First, in south-central Minnesota (one of the ovals in Fig. 3), the true observed visibility was unrestricted (10 miles). Using L21 (Fig. 3b) or the Equation 6 approach (Fig. 3c) leads to an underprediction of visibility in this area, while the RRFS approaches are closer to the observations (Fig. 3d, e). The second region, in southwestern Minnesota, highlights an area where visibility is substantially reduced due to BLSN in the observations (sites in this area were reporting haze at the time, but no snowfall). Neglecting the BLSN effect (Fig. 3a) leads to a dramatic overprediction of visibility here, while the four BLSN approaches capture the effect to varying degrees (Fig. 3b, c, d, e). The combination of 7-10 m s^{-1} 10-m wind speeds and low-density snow cover (Fig. 2) allows for a relatively accurate prediction of BLSN in this area. In contrast, the region highlighted in western North Dakota shows an area where the true visibility was reduced due to BLSN, but it is not captured well by any of the visibility approaches (Fig. 3b, c, d, e). This is because the RRFS has very light or nonexistent snow cover in this region, illustrating the dependence of the RRFS BLSN visibility forecasts upon accurate predictions of snow cover. It is also interesting to note that including a BLSN effect on the visibility (Fig. 3b, c, d, e) leads to improved forecasts (stronger reduction of visibility) in the area of active snowfall (Fig. 4) and strong winds in Iowa (Fig. 5) compared to the no-BLSN visibility diagnostic (Fig. 3a).

It was also found that the blowing snow reduction in visibility was far too high for forested areas. Generally, reduction in visibility from blowing snow generally does not occur in forested areas. Therefore, the BLSN term in equation 9 was made conditional to apply it only when local roughness length (determined from land-use classification; Smirnova et al. 2016, He et al 2021) was less than 0.7 m. The removal of BLSN effect in forested areas, shown in Fig. 3e, was in agreement with visibility observations in southwestern Ontario (upper right portion of the panel), and appears favorable in other cases, as well. Exclusion of forested areas for BLSN reduction in the diagnosed visibility is important for both surface transportation and airport operations.

This method was first tested with experimental HRRR postprocessing in August 2022. In winter 2023, it was refined and added to the Unified Post-Processing software (UPP) that will be

Accepted for publication in *Weather and Forecasting.* DOI 10.1175/WAF-D-23-0195.1.

used for post-processing in the RRFS. Testing of this BLSN visibility method using Equation 9 has continued since spring 2023 in the experimental version of RRFS running in real time.

d. A history-based snow driftability correction

In the initial RRFS tests with the framework developed in Section 2.c, the visibility reduction from BLSN was overpredicted in regions with a snow cover. As previously mentioned, the L21 framework assumes that the surface snow is perfectly driftable resulting in too much reduction in visibility especially in areas with old snow. In Section 2.c, we presented an effective parameter reduction in Equation (9) and in addition, incorporation of snow driftability through model-predicted snow density, which increases with age. We now discuss a different snowfall-history-based approach for estimating driftability, a method that focuses on the short-term history of snowfall.

The more intense BLSN events typically happen during snowstorms or within the first few hours after falling snow cessation (Baggaley and Hanesiak 2005). This is because (a) drifting snow builds a crust by breaking and compacting the ice crystals, (b) the readily driftable/blowable snow has been moved already to places from where it cannot be transported again (source depletion), and (c) older snow may experience vapor deposition and melt cycles, causing surface crusting. The first two processes are rapid (hours), the third more is slower (days). The driftability estimation using the prognostic snow density (Equation (7)) in the 2-layer snow model in HRRR, as described in section 2.b, does not incorporate the rapid processes (a and b) at the surface of the snowpack. The increase in HRRR snow density tends to be a slow process, highly influenced by the 24-hour cycle IMS assimilation.

To empirically capture the rapid processes (a and b), we chose to implement an additional driftability correction, using an hourly HRRR snowfall record for a given forecast period, which varies by case and is between 6 to 18 hours (HRRR only outputs forecasts up to 18 hours for hourly outputs except 00, 06, 12, 18 UTC, which go out to 48 hours).

Our equation for driftability, D is

$$D = \frac{\Sigma(\alpha_i p_i)}{\Sigma p_i} \tag{10}$$

where α_i is the weighting factor at hour *i*. That is, we consider the precipitation, p , at hour *i*, with the subscript *i* indicating the number of hours back from the target forecast time. At first we

Accepted for publication in *Weather and Forecasting*. DOI 10.1175/WAF-D-23-0195.1.

set α_i=1 at all times, i.e. the older snow is fully driftable. Then we reduce the weighting factors to account for two processes.

First, we consider the impact of recent skin temperatures exceeding 0°C. A skin temperature T_{skin} above 0°C results in an ice crust upon refreezing. T_{skin} is used rather than the 2 m air temperature, because the temperature at the snow surface matters, and net radiation can cause significant differences between the two temperatures. We apply the following for each i as the following piecewise function, where $T_{skin,i}$ is in units of °C:

$$\alpha_{i,i+1,\ldots,11} = \begin{cases} \alpha_{i,i+1,\ldots,11}, & T_{skin,i} < 0 \\ 0, & T_{skin,i} \geq 0 \end{cases} \quad (10a)$$

In other words, the fallen snow cannot contribute to the BLSN if it fell at or before a time when the skin temperature was above 0°C, as the re-freezing of meltwater will crust the surface snow. The variable for T_{skin} is found in the HRRR output. For simplicity, we will assume that once the snow has crusted, it cannot be blown. In other words, we set α_i to 0 for the earlier times (higher values of i), i.e., the snow that fell before the melting episode cannot be eroded. In reality, BLSN may still result from a crusted snowpack, but it requires a higher threshold friction velocity for saltation (Equation 1).

And second, we account for the recent history of wind or wind gusts, which deplete the source of snow (reservoir depletion). Thus $\alpha_{i,new}$ is calculated as $\alpha_{i,new} = \alpha_i g(U)$, where $g(U)$ is calculated as the following piecewise function:

$$g(U) = \begin{cases} 1, & U < 5.5 \\ 1 - \frac{U-5.5}{30-5.5}, & 5.5 \leq U \leq 30 \\ 0, & U > 30 \end{cases} \quad (10b)$$

where U is 10 m wind speed (units of m s^{-1}). The 10 m wind, and the 5.5 to 30 m s^{-1} wind bounds, are derived from Fig. 2 in Pomeroy et al. (1993).

The final expression for driftability D is Equation (10), with adjustments for α_i given in (10a) and (10b). This driftability D is then applied as a multiplier to the BLSN concentration in Equation (4), and then a new visibility is calculated for each weight method using Equation (6) with the HRRR-prognosed snow density. In the implementation, we used HRRR forecast hour 12 as the "current" time, so we had ready access to the relevant model output over the previous 11 hours. Driftability can be computed for any other forecast time, using any combination of previous HRRR hourly runs and previous forecast times.

Accepted for publication in *Weather and Forecasting*. DOI 10.1175/WAF-D-23-0195.1.

e. BLSN particle size distribution

As mentioned before, L21 assumes an average size (diameter) of BLSN particles of 60 μm. Few BLSN particle size measurements exist, yet it matters because it affects visibility reduction (Equation 9). Schmidt (1981; 1984) recorded size distributions of blowing ice particles with an optical counter capable of detecting particles as small as 60 μm. The mean (mode) particle size, measured at various heights up to 1 m above the snow surface, was ~150 μm (~100 μm), i.e., not much larger than the size threshold for this instrument. The size distribution decays rapidly with height (Schmidt 1984) because the particle fallspeed increases with size.

More advanced measurements (e.g., Nishimura and Nemoto 2005; Lawson et al. 2006) suggests that many smaller BLSN particles are present, not detectable with the earlier optical sizing instruments. This matters, because small particles also reduce visibility, since light transmission is proportional to the integrated surface area of the scatterers (not their volume), and thus very sensitive to the number concentration. Nishimura and Nemoto (2005) showed that the BLSN particle size distribution in the lowest 1 m closely match a gamma distribution, with an effective diameter close to ~150 μm. Montpetit et al. (2011) and Yu et. al. (2020) suggest that this value is actually about 1-2 orders of magnitude larger, especially under stronger winds. For this study, we assume an average diameter of 400 μm (radius of 200 μm), which seems to roughly fall in the range of most of the non-L21 studies at a height of 2 m AGL, but clearly more field observations of BLSN particle size distribution are needed.

f. History-based driftability diagnostic process and case studies

We assess the history-based driftability correction for BLSN visibility reduction (Section 2.d), using output from HRRR. To accomplish this, we select twelve different cases, six which were determined to have occurred without falling snow, and six that happened with falling snow. This determination was a subjective process, using newspaper articles and looking at observations from the NOAA NCEI dataset to focus on times where observed visibility was reduced, with recent winds and snowfall taken into consideration. For example, the times in the 13 Mar 2019 case were set with the observations of precipitation ending after 1400 UTC, but visibility was still under a mile (1609.3 m, the dashed line in Fig. 6) and winds were stronger than 10 m s^{-1}. Thus, this was classified as a BLSN case *with* falling snow. An 8-h forecast was deemed sufficient for the precipitation to happen in calculating *D* for this case. Several stations

Accepted for publication in *Weather and Forecasting*. DOI 10.1175/WAF-D-23-0195.1.

were examined during each case time to establish a forecast time and forecast length. The comparison between forecasted and observed visibility at each station pulls the values at the closest HRRR grid cell to the station coordinate (latitude and longitude).

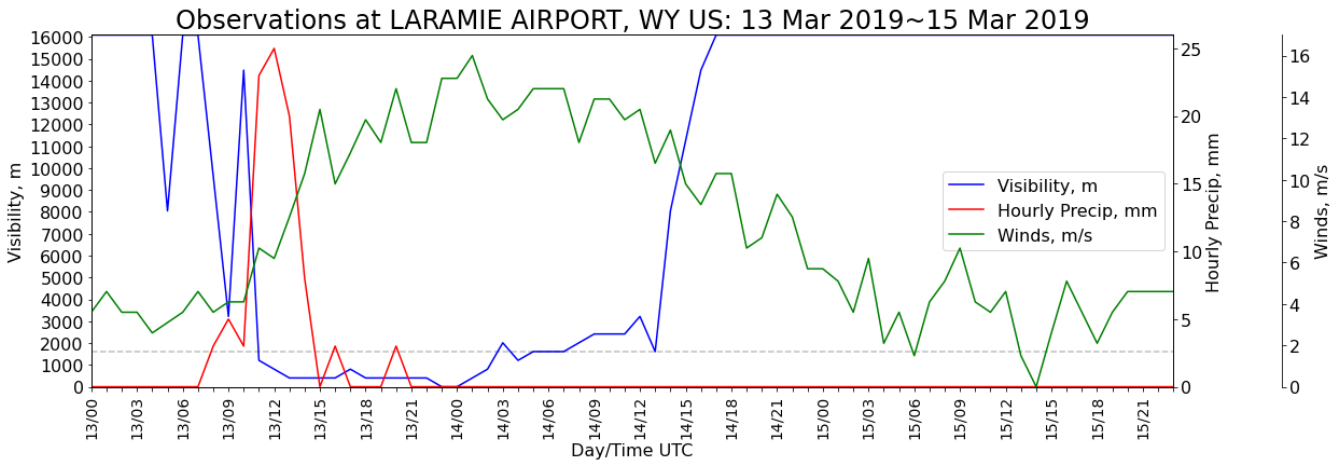

Fig 6: Observations at Laramie Airport from 13-15 Mar 2019 of visibility (blue), hourly precipitation (red), and winds (green).

The twelve cases are summarized in Table 1, with the study domain shown in Fig. 7.

Table 1: List of twelve BLSN cases used in this study. The valid forecast time (format: DD/MM HHMM, in UTC) is the time for which BLSN visibility reduction predictions are evaluated, and the forecast period (HH) is the model forecast hour (max. 18).

Valid Forecast Time (Forecast Period)	Concurrent Falling Snow?	General event summary
18 Nov 2018 1600 (12)	No	Isolated BLSN event, about 4 h long near Bordeaux, WY (KBRX; M. Brothers, Personal Communication).
13 Mar 2019 1400 (08)	Yes	This event was part of a “Bomb Blizzard” that affected much of eastern Wyoming and the Nebraska Panhandle (Cheyenne WFO 2019).
12 Dec 2019 2200 (10)	No	Recent snowfall of 20-38 cm (8-15”) with wind gusts exceeding 52 kts near Arlington, WY (KARL; Brothers et al. 2021).
31 Jan 2020 1600 (18)	No	Snow squall the night prior, with winds up to 39 kts shortly after near Vedauwoo, WY (KVDW; Brothers et al. 2021).

Accepted for publication in *Weather and Forecasting*. DOI 10.1175/WAF-D-23-0195.1.

14 Mar 2021 1000 (10)	Yes	25-35 cm (10-14”) snow in 6 h or less along Laramie Range, followed by strong winds about 39-48 kts and light snowfall along the Laramie Range (Cheyenne WFO 2021).
14 Mar 2021 1800 (18)	No	See above. The 14 Mar 2021 event was significant enough to warrant two different case times.
6 Jan 2022 2200 (10)	Yes	After a winter storm hit Central and Southern Wyoming, winds gusted up to 30 mph in Casper and 60 mph in Cheyenne, closing parts of I-80 and I-25 (Oil City Staff 2022).
15 Dec 2022 1600 (18)	No	Gillette received snow 3 days in a row with sustained winds around 10-17 kts and gusts up to 26 kts (Byrd 2022).
22 Feb 2023 1200 (12)	Yes	Up to 25 cm (10”) new snow in the eastern part of the state with wind gusts 20-30 mph (Day 2023)
4 Apr 2023 0800 (18)	Yes	60-75 cm (24-30”) in parts of eastern WY and southwest SD, winds gusting up to 35 kts behind the snowfall. I-80 and I-90 were closed for this storm (Corr 2023 and Rapid City WFO 2023a).
24 Nov 2023 2000 (18)	No	Central WY received between 25-60 cm (10-24”) of snow with Southern WY receiving slightly less (Rossi, 2023) with winds around 30-40 mph in Central WY (Byrd 2023a) and 40-50 in southeast WY (Byrd 2023b)
26 Dec 2023 1200 (06)	Yes	Most of Southeast WY was under some form of winter advisory, with high wind warnings mixed in (Cappucci 2023). 50-60 mph gusts were observed into northwestern SD (Rapid City WFO 2023b).

Because the purpose is to apply some driftability estimate eventually for operational forecasting, we run each case with an initialization time 6-18 h prior to each case study time, depending on the case (e.g., the 13 Mar 2019 1400 UTC case was an 8-h forecast with an initialization time of 13 Mar 2019 0600 UTC). The BLSN concentration and visibility attenuation then were calculated in the post-processing using the framework mentioned in Sections 3.b (which assumes D =1) and 3.d (with variable driftability). For testing purposes, the visibility output is either the HRRR baseline visibility value (without the BLSN framework), a combined visibility value assuming D = 1 (with the BLSN framework but excluding the driftability parameter), or a combined visibility value with variable driftability (with the BLSN framework including D). While we analyzed all twelve cases, we will only show figures and event summaries from two of

Accepted for publication in *Weather and Forecasting.* DOI 10.1175/WAF-D-23-0195.1.

the case studies here, one without falling snow (24 Nov 2023 2000 UTC) and one with falling snow (13 Mar 2019 1400 UTC). The remaining ten cases are summarized in the Supplement. Our domain of focus is centered on Wyoming, but includes parts of surrounding states, specifically, the domain contains the longitude range of 112°W to 103°W and the latitude range of 40°N to 46°N (hereafter WY Plus domain) (Fig. 7).

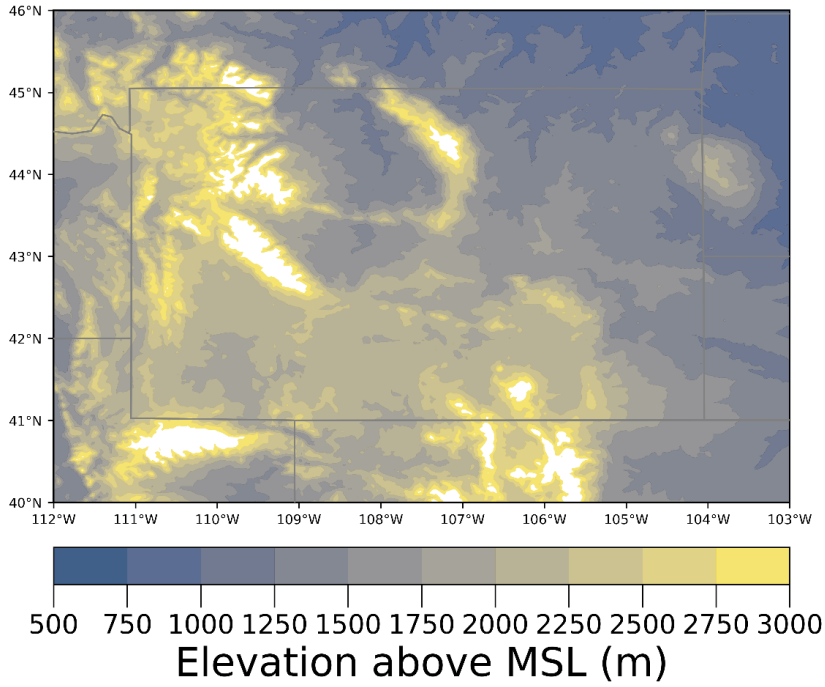

Fig. 7. The WY Plus domain with terrain elevation. White areas indicate elevation > 3000 m.

g. Validation

The surface visibility observations used to validate the model are again from ASOS stations as used in Fig. 3. The predicted visibility is at 2 m AGL. The height AGL of the ASOS visibility sensors is generally above 2 m and varies from station to station (NOAA 1998). Ideally, we "correct" the ASOS visibility to 2 m using the height-dependent BLSN concentration (Equation 4). Unfortunately, visibility sensor height information is not available in the station description or metadata. According to the ASOS manual (FAA 2017), the recommended height is between 2.4-3.7 m AGL, and at least 1.8 m above the maximum snow depth recorded at the area. We acknowledge that the comparison between the predicted visibility and the ASOS visibility is imperfect, and that a negative bias in the predicted visibility may be due simply to the height of the ASOS visibility sensors, which are generally above 2 m. For instance, under

Accepted for publication in *Weather and Forecasting*. DOI 10.1175/WAF-D-23-0195.1.

BLSN conditions, a visibility of 5 km measured at 3 m AGL converts to a visibility of about 4.1 km (6.1 km) at 2 m (5 m) AGL, respectively, according to Equations (4) – (6). We could also validate BLSN presence using webcam imagery (McCorkle 2021), or, for extreme events, satellite imagery (L21), but, since these measurements do not quantify visibility reduction, they are beyond the scope of this study.

The National Centers for Environmental Information (NCEI) data collects and archives observations from ASOS and state DOT stations, including visibility. We collect all these observations within our domain and compare them to the closest HRRR grid point. Contingency tables are developed for different visibility thresholds: 10 mi, < 5 mi, < 3 mi, < 1 mi, and <½ mi (16 km, 8 km, 4.8 km, 1.6 km, and 0.8 km, respectively). We then calculate the Heidke Skill Score (HSS) as described in Equation (6) of Hyvärinen (2014). This is done for the five threshold visibilities and with HRRR visibility, then BLSN with/without driftability correction for a total of 15 contingency tables.

3. Results

a. Case studies

i. 13 MAR 2019 at 1400 UTC

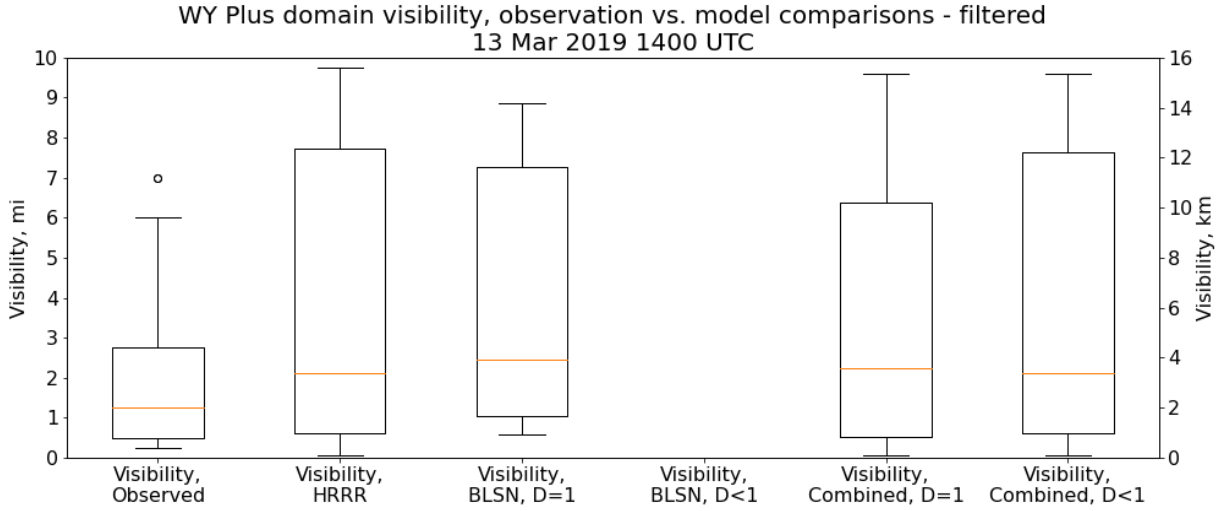

Fig. 8. Visibility distribution (miles on left, km on right axis) for the case valid 13 Mar 2019 at 1400 UTC, showing, from left to right, visibility distributions of Observed, HRRR/no BLSN, Only BLSN, full driftability assumption, Only BLSN with driftability calculations, HRRR+BLSN (Combined) visibility with full driftability assumption, and HRRR+BLSN (Combined) visibility with driftability calculations. Any visibility values ≥ 10 mi (16 km) are filtered out.

Accepted for publication in *Weather and Forecasting*. DOI 10.1175/WAF-D-23-0195.1.

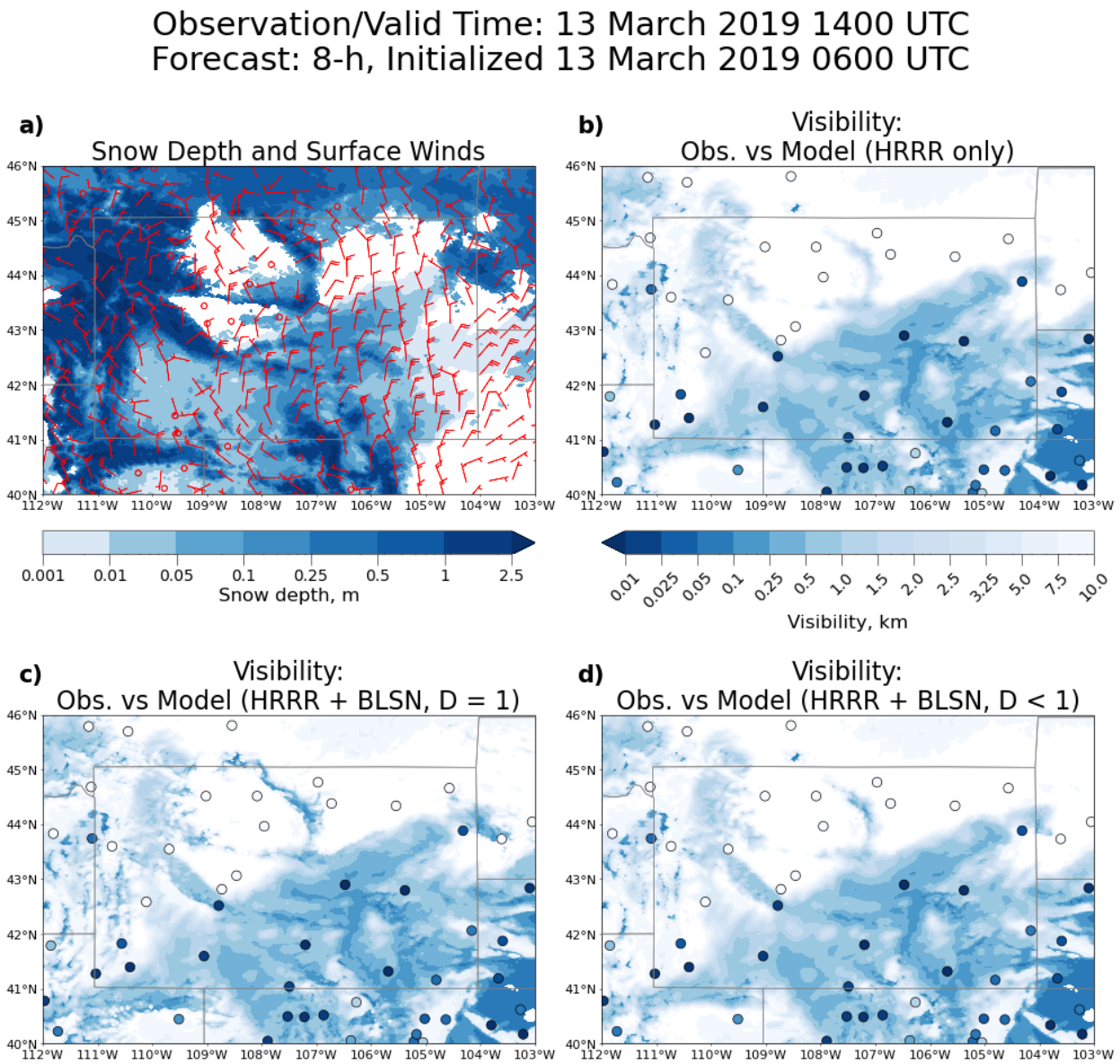

Fig. 9. (a) Snow depth (color) and surface winds, then (b)-(d) visibility station observations in filled circles compared to (b) HRRR forecast only (i.e. no BLSN), (c) HRRR with BLSN at D = 1 (i.e. BLSN but assume full driftability as the original L21 framework, and (d) HRRR with BLSN and D < 1 (i.e. applying driftability formula to the original L21 framework) for valid time 13 March 2019 1400 UTC. Panel (a) uses the snow depth color bar and (b)-(d) use the visibility color bar.

For the 13 March 2019 case, much of Wyoming either received snow from the bomb blizzard that happened, or it was already there from earlier in the season, though given the HRRR visibility (no BLSN) panel (b) in Figure 9, it's likely the former. Figure 8 shows that after

Accepted for publication in *Weather and Forecasting*. DOI 10.1175/WAF-D-23-0195.1.

applying our driftability formula, there are no BLSN-only visibilities under 16 km (10 mi) which results in panel (d) in Figure 9 looking very similar to panel (b). The one exception is a streak in north central WY. Unfortunately, the spatial resolution of observations does not pick that up. When comparing forecasted visibility to observed visibility, in general, the two line up well, but forecasted visibilities in southern WY are generally higher than observed. The one area that is completely missed is southwest WY corner. Unfortunately, this is around where I-80 is and may have been a bad missed forecast. Overall, it seems like BLSN was not a huge factor in reduced visibilities like originally thought.

ii. 24 NOV 2023 at 2000 UTC

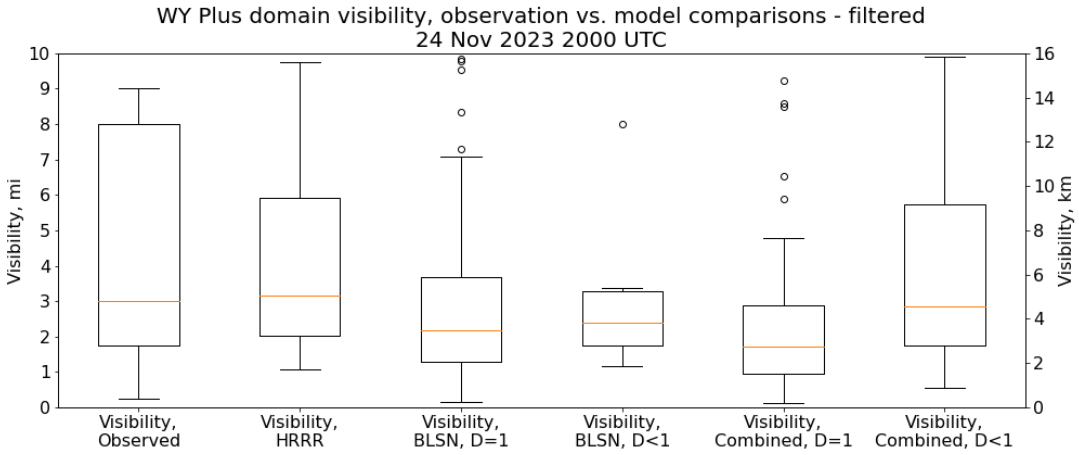

Fig. 10. As in Fig. 8, but for valid time 24 Nov 2023 at 2000 UTC.

Accepted for publication in *Weather and Forecasting*. DOI 10.1175/WAF-D-23-0195.1.

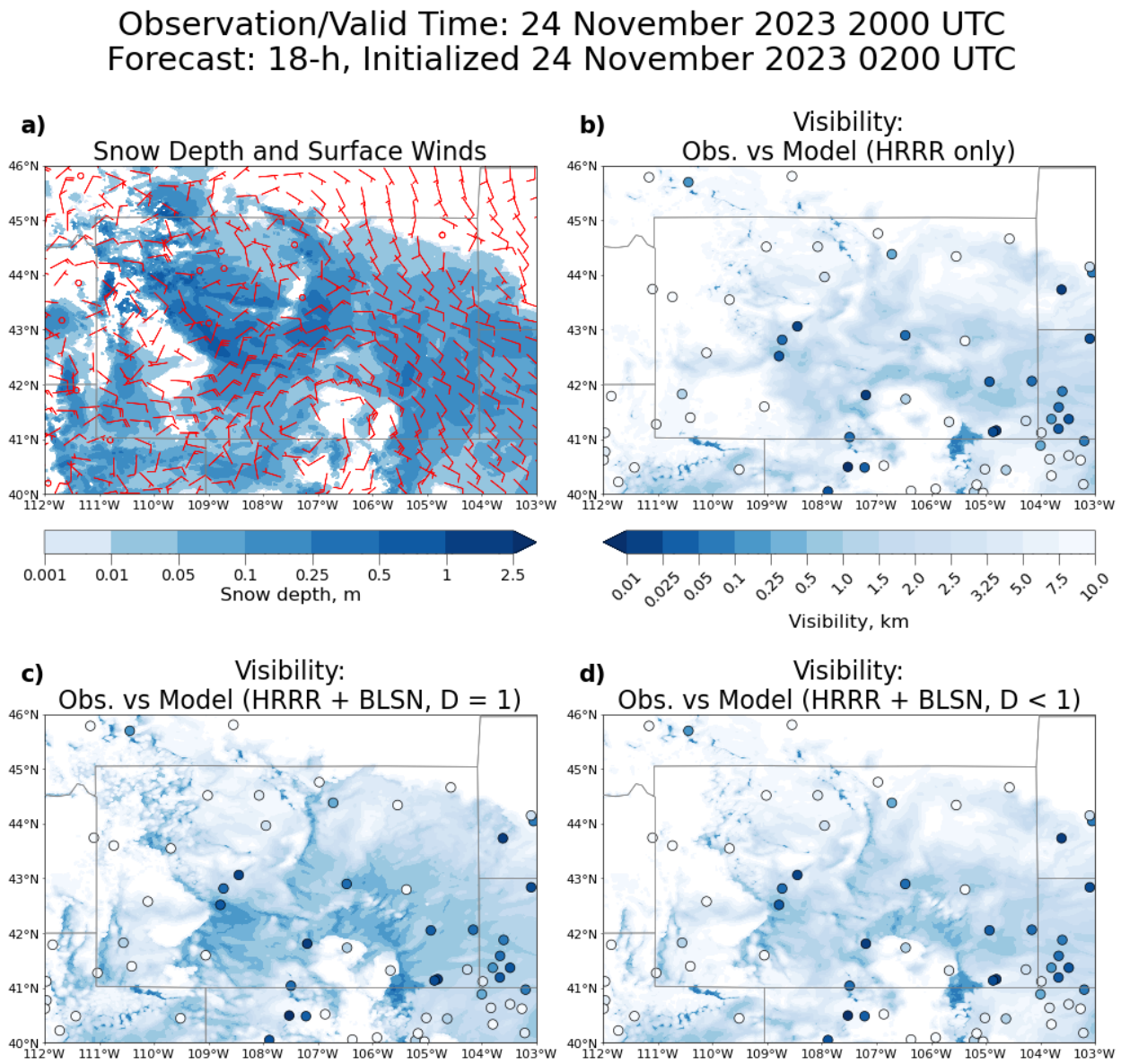

Fig 11: As in Fig. 9, but for valid time 24 Nov 2023 at 2000 UTC.

Like the 13 March 2019 case, much of WY has at least some snow cover, even though it's only November. However, unlike the 13 March 2019, the HRRR forecasted visibility (Figure 11, panel b) severely overpredicts visibility when compared to observations, especially in central WY, where observed visibilities are well under 0.5 km but forecasted visibilities range from 1.5 to 5 km. Adding BLSN to the forecast (Figure 11, panel c) does get these forecasts closer to observations, especially in the central part of the state. Once we apply the driftability parameter (Figure 11, panel d), we are left with thin, dark scattered streaks (this is most apparent from 109

Accepted for publication in *Weather and Forecasting*. DOI 10.1175/WAF-D-23-0195.1.

°W to 107 °W). Additionally, the high forecasted visibility pocket in the south-central part of the state closely aligns with higher visibility observations, and the lower forecasted visibility surrounding that pocket match observations of lower visibilities outside the pocket. These streaks line up with forested mountains in southern WY and in northern WY. Over these forests, dominated by evergreen trees (mostly Lodgepole and Ponderosa pine), the roughness length far exceeds that of any kind of snow (~0.5 m for forests vs ~0.003 m for snow (Saheb et al. 2014)). The ~three orders of magnitude increase in surface roughness over forests means that, according to Equation 1, Q_s may be mathematically < 0, thus physically 0. Meteorologically, this means it is very difficult for BLSN to occur in forests, which is consistent with Fig. 1. Figure 10 shows that applying BLSN and the driftability parameter to visibility forecasts are necessary in this case. After filtering out visibilities > 16 km (10 mi), the mean visibility in each case remains around 3-5 km (2-3 mi).

b. Validation

As mentioned in Section 3.f, the visibility was calculated in HRRR post-processing using the framework mentioned in Section 3.b, which assumes *D* =1, and in Section 3.d, which introduced the history-based variable snow driftability. We now validate the computed visibility against ASOS station observations, not as a scatterplot, but rather in the form of five different threshold visibilities that are commonly used by the NWS, i.e. 10, 5, 3, 1, and 0.5 miles. The question we ask is: how well do the four methods predict reduced visibility for the five different severity thresholds? The verification scores for each simulation are shown in Tables 2-4, separated by case type.

Table 2. Verification scores for five commonly used visibility thresholds, using the Heidke Skill Score (HSS). Shown is the original HRRR visibility (HRRR) not including BLSN, FULL, which assumes full driftability (*D*=1), and NOTFULL, which is the history-based driftability method. Includes all cases.

All Cases	**HSS**		
Visibility Threshold	HRRR	FULL	NOTFULL
> 16 km (10 mi)	0.499	0.461	0.490
< 8 km (5 mi)	0.646	0.527	0.609
< 4.8 km (3 mi)	0.660	0.572	0.653
< 1.6 km (1 mi)	0.530	0.434	0.536
< 0.8 km (0.5 mi)	0.461	0.374	0.459

Accepted for publication in *Weather and Forecasting*. DOI 10.1175/WAF-D-23-0195.1.

Table 3. As in Table 2, for BLSN cases without falling snow only.

Cases w/out falling snow	**HSS**		
Visibility Threshold	HRRR	FULL	NOTFULL
> 16 km (10 mi)	0.490	0.424	0.481
< 8 km (5 mi)	0.632	0.472	0.585
< 4.8 km (3 mi)	0.571	0.475	0.593
< 1.6 km (1 mi)	0.543	0.381	0.569
< 0.8 km (0.5 mi)	0.463	0.492	0.463

Table 4. As in Table 3, for BLSN cases with falling snow only.

Cases with falling snow	**HSS**		
Visibility Threshold	HRRR	FULL	NOTFULL
> 16 km (10 mi)	0.460	0.456	0.452
< 8 km (5 mi)	0.618	0.529	0.587
< 4.8 km (3 mi)	0.677	0.606	0.657
< 1.6 km (1 mi)	0.497	0.434	0.495
< 0.8 km (0.5 mi)	0.454	0.297	0.451

Each of the three columns in Tables 2-4 are compared to station observations. Overall, the HSS from HRRR to FULL showed decreases (significant or not) in HSS in every comparison except one, while FULL to NOTFULL showed increases (significant or not) in HSS, but the HSS and NOTFULL scenarios present similar HSSs (i.e. the differences are not statistically significant). There is one exception to this, which is the < 0.8 km threshold in cases without falling snow. Here, the HSS increased when comparing HRRR to FULL (0.039 increase) and decreased from FULL to NOTFULL (0.039 decrease). In short, *the history-based driftability approach generally improves the BLSN visibility reduction predictive skill from the original L21 framework, but the improvements are not significant on average and do not improve when compared to the HRRR visibility, thus rendering the case-by-case results inconclusive.*

4. Discussion

a. Snow driftability and BLSN visibility reduction predictability

The driftability calculations explained in Section 3.b, building on L21, provide a first-guess BLSN concentration profile used to estimate visibility reduction. We then introduced a

Accepted for publication in *Weather and Forecasting*. DOI 10.1175/WAF-D-23-0195.1.

correction based on predicted time-varying snow density from the land-surface model (Section 2.c), and then a further correction to account for the fact that not all snow on the ground is fully driftable (also in section 2.c). Our history-based quantification of driftability lacks empirical evidence that can be integrated in an operational NWP model such as HRRR or RRFS. First, we assume all snow older than our forecast period (case dependent, ranging from 6-18 hours) is not driftable. To a first-order, the majority of BLSN events occur within the first hour or two of snowfall cessation (Baggaley and Hanesiak 2005), but that doesn't mean these events can't occur with older snow; in fact, BLSN events do occur well after snowfall ends given extremely cold air, cold snowpack temperatures, and little wind during the period from the snowfall cessation to the BLSN event (Baggaley and Hanesiak 2005). Second, the wind history is assumed in this study to have a linear effect on the driftability of snow from 5.5 m s^{-1} to 30 m s^{-1}, but this may not be realistic, as suggested by Pomeroy et al. (1993, their Fig. 2). The lower bound of 5.5 m s^{-1} may be rather robust, but the upper bound of 30 m s^{-1} is an extrapolation. Third, the depletion term from historical winds in α_i itself does not factor the amount of blowable snow and may artificially stop driftability when there is still more depletable snow. And there are several other assumptions, including the BLSN gamma particle size distribution, the mean particle radius, and the credibility of the power law assumption in Equation (5).

In short, model output based *BLSN predictability can benefit from targeted observational studies*, especially sensitivity tests on mean particle radius, which has been shown to have an impact on visibility estimates (e.g. L21). Additionally, Wyoming does not have many station observations of visibility; way too few to match the 3-km grid spacing of the HRRR and RRFS. Theoretically, the simplest solution is to add more visibility sensors throughout the state. Adding these near state highway and interstate mile markers would be a great start. Realistically, this might not be feasible, likely due to the cost of these sensors and the increased maintenance that would have to happen.

Other approaches are possible. Driftability could also be quantified by assuming a variable threshold friction velocity ($\boldsymbol{u_{*t}}$). In most surface layer parameterizations, friction velocity $\boldsymbol{u_*^2 = C_M U^2}$, where U is the 10 m wind speed and $\boldsymbol{C_M}$ the drag coefficient, which depends on static stability. Thus, $\boldsymbol{u_{*t}}$ in Equation (1) is proportional to the minimum wind speed needed to begin to pick up the snow. The higher $\boldsymbol{u_{*t}}$, the less driftable the snow is. In this study,

Accepted for publication in *Weather and Forecasting*. DOI 10.1175/WAF-D-23-0195.1.

we used the same constant value as in L21 ($\boldsymbol{u_{*t}}$ =0.2 m s^{-1}). This value of $\boldsymbol{u_{*t}}$ is representative of fresh snow over bare land (no vegetation above the snow layer). Driftability can be tuned as a function of a variable $\boldsymbol{u_{*t}}$ (e.g., He and Ohara 2017): some snowpack models include snow shapes/shape parameters to quantify the driftability of snow (e.g., Vionnet et al. 2012), and $\boldsymbol{u_{*t}}$ can be expressed as a function of snow shape (He and Ohara 2017). The HRRR model physics do not include a surface snow shape parameter, but this could be implemented in the future.

Given the sensitivity of $\boldsymbol{C_r}$ (or $\boldsymbol{Q_s}$, Equation 2) and driftability to instantaneous wind speed (rather than just the mean wind speed), the fluctuations in BLSN concentrations may be larger than the mean value in Equation (4), especially in gusty conditions. Eddy fluctuations are essential for the vertical transport of BLSN in the surface layer, but they are ignored in this study. Since the visibility calculation essentially integrates over many eddies, this limitation may be less severe, but still, large variations in visibility may occur in BLSN conditions, as frequent motorists surely have experienced, especially if these eddies cause an overall increase in particles at higher heights.

b. Limitations in NOAA operational model implementation

By March 2023, the NOAA Unified Post-Processor (UPP) for the experimental RRFS post-processing contained a working model of the BLSN visibility reduction framework discussed in Section 2.b and 2.c leading up to Equation (9). The HRRR and RRFS are 3-km, convection permitting weather models with output every 15 minutes. These models have several shortcomings when it comes to forecasting BLSN visibility. First, the spatial scales of the HRRR and RRFS limit local details on BLSN and will not capture small-scale convective rolls sometimes important for BLSN events with reduced visibility (Kennedy and Jones 2020, Kennedy et al 2022). While these models are high-resolution, BLSN may be highly variable on subgrid scales (i.e. < 3 km), certainly in complex terrain or heterogenous land cover. Second, HRRR and RRFS processing is such that "history" model output to calculate driftability is not readily available. Thus, we need to introduce variables to the system that would help these models better represent driftability, and in turn, BLSN visibility. For that reason, only the modified BLSN visibility calculation using Equation (9) using prognostic snow density is now used in the experimental RRFS, not the history-based BLSN driftability method (Section 2.d). Future research can also consider the snow shape parameter, which is detailed in section 3 of

Accepted for publication in *Weather and Forecasting.* DOI 10.1175/WAF-D-23-0195.1.

Vionnet et al. (2012). This algorithm calculates driftability based on the snow shape (dendritic vs non-dendritic), which depends on wind speed and air temperature. While Vionnet et al. (2012) do not specify the level of wind measurement, standard levels (10 m wind speed and 2 m temperature) can be used in that framework. This will help keep in line with the diagnostic nature of the operational models. More empirical studies of top-layer snow-to-liquid ratio (SLR) (Alcott and Steenburgh 2010) and snow surface crusting would be helpful. Fresh-snow densities are a factor of snow crystal shape, cloud-level air temperature, and liquid/supercooled liquid water content, and can vary from about 10 to 350 kg m^{-3} (Judson and Doesken 2000). Additionally, the snow model in Vionnet et al. (2012) has time-dependent expressions for the density of the snowpack and the top layer of snow.

Other models for blowing snow have been coupled to atmospheric prediction models such as WRF, including a column BLSN model which was tested in the field (Kennedy et al 2022), and several surface snow models with more comprehensive snowpack dynamics including BLSN, such as WRF-ice (Luo et al. 2020) and CRYOWRF (Gerber et al. 2023). None of these models are truly comprehensive and broadly applicable, e.g. CRYOWRF struggles with the presentation of BLSN + falling snow. The main challenge remains the lack of empirical data to quantify age-dependent driftability as a function of model-resolved parameters.

5. Conclusions

This study aimed to improve the visibility diagnostic used in the HRRR and RRFS weather prediction models by adding visibility attenuation due to BLSN. A recently developed diagnostic framework for forecasting blowing snow concentration and the associated visibility reduction, developed by L21, was applied to HRRR model output including land-surface conditions to improve the visibility diagnostic in the presence of BLSN. The key conclusions are as follows:

- The original L21 visibility reduction due to BLSN was too aggressive in areas of older snow, on account of the assumption of full driftability of the snowpack.
- A first-order driftability reduction based on time-varying snowpack density from the RUC land surface model used in HRRR and RRFS was evaluated in RRFS and is now incorporated in the real-time UPP of the experimental RRFS.

Accepted for publication in *Weather and Forecasting.* DOI 10.1175/WAF-D-23-0195.1.

- A second, complementary, process-based method to estimate snowpack driftability required data for recent (6-18 h) snowfall, wind speed, and skin wet-bulb temperature. This method was tested using twelve blowing snow events around Wyoming from 2018 to 2023. Six include falling snow, and six exclude falling snow. Compared to the full driftability assumption, this method showed little, possibly insignificant, improvements.
- To make further progress with the model-based diagnosis of blowing-snow-induced visibility reductions, more empirical work is needed to determine the relation between snowpack driftability and the recent history of snowfall and other weather conditions.
- The BLSN diagnostic term for visibility was also modified to apply only for areas with roughness length less than 0.7 m, thus excluding forested areas.

Acknowledgments. Tim Corrie, Bart Geerts, and Zach Lebo acknowledge support from NOAA CSTAR grant #NA19NWS4680005. Additionally, Tim Corrie acknowledges support from NOAA Cooperative Agreement for CIRES grant #NA17OAR4320101. The NOAA CSTAR grant funded the research approach (Section 2.d), while the NOAA Cooperative Agreement for CIRES funded the operational approach (Section 2.c). This study benefitted from discussions with Ted Letcher, the three reviewers (Aaron Kennedy plus two anonymous reviewers), Noriaki Ohara, Trevor Alcott, and several NWS forecasters, including Chris Hammer and Rob Cox.

Data availability statement

The HRRR data were obtained from Amazon Web Services at https://noaa-hrrr-bdp-pds.s3.amazonaws.com/index.html using jupyterhub and the wget command. The RRFS experimental visibility diagnostic products including BLSN effects can be accessed from http://rapidrefresh.noaa.gov/RRFS. Code used to create the figures shown in section 3 and in the supplemental material are available upon request.

Accepted for publication in *Weather and Forecasting.* DOI 10.1175/WAF-D-23-0195.1.

References

Alcott, T. I., and W. J. Steenburgh, 2010: Snow-to-Liquid Ratio Variability and Prediction at a High-Elevation Site in Utah's Wasatch Mountains. *Weather and Forecasting*, **25**, 323–337, https://doi.org/10.1175/2009WAF2222311.1.

Atmospheric Environment Service, 1977: *Manual of Surface Weather Observations (MANOBS)*. 7th ed. Atmospheric Environment, 322 pp.

Baggaley, D. G., and J. M. Hanesiak, 2005: An Empirical Blowing Snow Forecast Technique for the Canadian Arctic and the Prairie Provinces. *Weather and Forecasting*, **20**, 51–62, https://doi.org/10.1175/WAF-833.1.

Benjamin, S. G., and Coauthors, 2004: An hourly assimilation–forecast cycle: The RUC. *Mon. Wea. Rev.*, **132**, 495–518, https://doi.org/10.1175/1520-0493(2004)132<0495:AHACTR>2.0.CO;2

——, 2016: A North American hourly assimilation and model forecast cycle: The Rapid Refresh. *Mon. Wea. Rev.*, **144**, 1669-1694. http://dx.doi.org/10.1175/MWR-D-15-0242.1

——, 2021: Diagnostic fields developed for hourly updated NOAA weather models. NOAA Tech. Memo. OAR GSL-66, https://doi.org/10.25923/F7B4-RX42.

——, T. G. Smirnova, E. P. James, L.-F. Lin, M. Hu, D. D. Turner, and S. He, 2022: Land–snow data assimilation including a moderately coupled initialization method applied to NWP. *Journal of Hydrometeorology*, **23**, 825–845, https://doi.org/10.1175/JHM-D-21-0198.1.

Bringi, V., M. Grecu, A. Protat, M. Thurai, and C. Klepp, 2021: Measurements of Rainfall Rate, Drop Size Distribution, and Variability at Middle and Higher Latitudes: Application to the Combined DPR-GMI Algorithm. *Remote Sensing*, **13**, 2412, https://doi.org/10.3390/rs13122412.

Brothers, M. R., R. Cox, B. Geerts, Z. Lebo, S. McCorkle, and R. Capella, 2021: Evaluation of Current National Weather Service Blowing Snow Forecasting Techniques across Southeast Wyoming. 20th Conf. on Artificial Intelligence for Environmental Science Artificial Intelligence for High-impact Weather, Virtual event https://ams.confex.com/ams/101ANNUAL/meetingapp.cgi/Paper/379667.

Bruland, O., Å. Færevåg, I. Steinsland, G. E. Liston, and K. Sand, 2015: Weather SDM: estimating snow density with high precision using snow depth and local climate. *Hydrology Research*, **46**, 494–506, https://doi.org/10.2166/nh.2015.059.

Accepted for publication in *Weather and Forecasting*. DOI 10.1175/WAF-D-23-0195.1.

Burrows, W. R., and C. J. Mooney, 2021: Blizzard Conditions in the Canadian Arctic: Observations and Automated Products for Forecasting. *Weather and Forecasting*, https://doi.org/10.1175/WAF-D-20-0077.1.

Byrd, K., 2022: Winter storm dumps more than 21 inches of snow; blowing snow, wind main concerns today. https://county17.com/2022/12/16/winter-storm-dumps-more-than-21-inches-of-snow-blowing-snow-wind-main-concerns-today/ (Accessed May 22, 2023).

——, 2023a, Oil City News: Winter storm warning continues for Casper; below-normal temps set in. https://oilcity.news/community/weather/2023/11/24/winter-storm-warning-continues-for-casper-below-normal-temps-set-in/ (Accessed March 18, 2024).

——, 2023b, Cap City News: Winter storm warning continues for Cheyenne; below-normal temps set in. https://capcity.news/weather-2/2023/11/24/winter-storm-warning-continues-for-cheyenne-below-normal-temps-set-in/ (Accessed March 18, 2024).

Cappucci, M., 2023: Blizzard and ice storm slam northern Plains, snarl travel. https://www.washingtonpost.com/weather/2023/12/26/blizzard-ice-storm-northern-plains-travel/ (Accessed March 18, 2024).

Cheyenne, WY WFO, 2019: March 13 and 14 2019 Blizzard. https://www.weather.gov/cys/March13142019Blizzard. (Accessed March 18, 2024).

——, 2021: Historic March Blizzard of 2021. https://www.weather.gov/cys/HistoricMarch2021Blizzard. (Accessed May 22, 2023).

Chritin, V., R. Bolognesi, and H. Gubler, 1999: FlowCapt: a new acoustic sensor to measure snowdrift and wind velocity for avalanche forecasting. *Cold Regions Science and Technology*, **30**, 125–133, https://doi.org/10.1016/S0165-232X(99)00012-9.

Corr, W., 2023: Cowboy State Daily. *Don Day Wyoming Weather Forecast: Tuesday, April 4, 2023*,. https://cowboystatedaily.com/2023/04/04/don-day-wyoming-weather-forecast-tuesday-april-4-2023/ (Accessed May 22, 2023).

Day, D., 2023: Cowboy State Daily. *Don Day Wyoming Weather Forecast: Wednesday, February 22, 2023*,. https://cowboystatedaily.com/2023/02/22/don-day-wyoming-weather-forecast-wednesday-february-22-2023/ (Accessed March 18, 2024).

Déry, S. J., and M. K. Yau, 1999: A climatology of adverse winter-type weather events. *J. Geophys. Res.*, **104**, 16657–16672, https://doi.org/10.1029/1999JD900158.

Accepted for publication in *Weather and Forecasting*. DOI 10.1175/WAF-D-23-0195.1.

Dowell, D. C., and Coauthors, 2022: The High-Resolution Rapid Refresh (HRRR): An Hourly Updating Convection-Allowing Forecast Model. Part I: Motivation and System Description. *Weather and Forecasting*, **37**, 1371–1395, https://doi.org/10.1175/WAF-D-21-0151.1.

Federal Aviation Administration, 2017: *Siting Criteria for Automated Weather Observing Systems*. https://www.faa.gov/documentLibrary/media/Order/6560_20c_ord.pdf.

FHWA 2016: The 2016 Traffic Monitoring Guide. Federal Highway Administration. Available at https://www.fhwa.dot.gov/policyinformation/tmguide/

Geerts, B., B. Pokharel, and D. A. R. Kristovich, 2015: Blowing Snow as a Natural Glaciogenic Cloud Seeding Mechanism. *Mon. Wea. Rev.*, **143**, 5017–5033, https://doi-org/10.1175/MWR-D-15-0241.1

Gerber, F., V. Sharma, and M. Lehning, 2023: CRYOWRF—Model Evaluation and the Effect of Blowing Snow on the Antarctic Surface Mass Balance. *JGR Atmospheres*, **128**, e2022JD037744, https://doi.org/10.1029/2022JD037744.

Greeley, R., and J. D. Iversen, 1985: *Wind as a Geological Process: On Earth, Mars, Venus and Titan*. 1st ed. Cambridge University Press.

Guyomarc'h, G., and L. Mérindol, 1998: Validation of an application for forecasting blowing snow. *Ann. Glaciol.*, **26**, 138–143, https://doi.org/10.3189/1998AoG26-1-138-143.

He, S., and N. Ohara, 2017: A New Formula for Estimating the Threshold Wind Speed for Snow Movement. *J. Adv. Model. Earth Syst.*, **9**, 2514–2525, https://doi.org/10.1002/2017MS000982.

He, S., T. G. Smirnova, S.G. Benjamin, 2021: Single-Column Validation of a Snow Subgrid Parameterization in the Rapid Update Cycle Land-Surface Model (RUC LSM). *Wat. Res. Research*, 57(8), e2021WR029955, https://doi.org/10.1029/2021WR029955

Horvath, H., 1971: On the applicability of the koschmieder visibility formula. *Atmospheric Environment (1967)*, **5**, 177–184, https://doi.org/10.1016/0004-6981(71)90081-3.

Huang, Q., J. Hanesiak, S. Savelyev, T. Papakyriakou, and P. A. Taylor, 2008: Visibility during Blowing Snow Events over Arctic Sea Ice. *Weather and Forecasting*, **23**, 741–751, https://doi.org/10.1175/2008WAF2007015.1.

Huo, X., N. Huang, and J. Zhang, 2022: A Numerical Research on the Relationship between Aeolian Sand Ripples and the Sand Flux. *Processes*, **10**, 354, https://doi.org/10.3390/pr10020354.

Accepted for publication in *Weather and Forecasting*. DOI 10.1175/WAF-D-23-0195.1.

Hyvärinen, O., 2014: A Probabilistic Derivation of Heidke Skill Score. *Weather and Forecasting*, **29**, 177–181, https://doi.org/10.1175/WAF-D-13-00103.1.

James, E. P., and Coauthors, 2022: The High-Resolution Rapid Refresh (HRRR): An Hourly Updating Convection-Allowing Forecast Model. Part II: Forecast Performance. Wea. Forecasting, 37, 1397–1417, https://doi.org/10.1175/WAF-D-21-0130.1

Judson, A., and N. Doesken, 2000: Density of Freshly Fallen Snow in the Central Rocky Mountains. *Bull. Amer. Meteor. Soc.*, **81**, 1577–1587, https://doi.org/10.1175/1520-0477(2000)081<1577:DOFFSI>2.3.CO;2.

Kennedy, A., and C. Jones, 2020: GOES-16 observations of blowing snow in horizontal convective rolls on 24 February 2019. *Mon. Wea. Rev.*, **148**, 1737– 1750. https://doi.org/10.1175/MWR-D-19-0354.1.

Kennedy, A. and Coauthors, 2022: Bringing microphysics to the masses: The Blowing Snow Observations at the University of North Dakota: Education through Research (BLOWN-UNDER) Campaign. *Bull. Amer. Meteor. Soc.*, **103**, E83-E100. https://doi.org/10.1175/BAMS-D-20-0199.1.

Lawson, R. P., B. A. Baker, P. Zmarzly, D. O'Connor, Q. Mo, J.-F. Gayet, and V. Shcherbakov, 2006: Microphysical and Optical Properties of Atmospheric Ice Crystals at South Pole Station. *Journal of Applied Meteorology and Climatology*, **45**, 1505–1524, https://doi.org/10.1175/JAM2421.1.

Letcher, T. W., S. L. LeGrand, and C. Polashenski, 2021: Applying a Physically Based Blowing Snow Diagnostic Parameterization to Improve Wintertime Visibility Forecasts in the WRF Model. *Weather and Forecasting*, **36**, 615–626, https://doi.org/10.1175/WAF-D-20-0106.1.

Liston, G. E., and M. Sturm, 1998: A snow-transport model for complex terrain. *J. Glaciol.*, **44**, 498–516, https://doi.org/10.3189/S0022143000002021.

Luo, L., J. Zhang, R. Hock, and Y. Yao, 2021: Case Study of Blowing Snow Impacts on the Antarctic Peninsula Lower Atmosphere and Surface Simulated With a Snow/Ice Enhanced WRF Model. *JGR Atmospheres*, **126**, e2020JD033936, https://doi.org/10.1029/2020JD033936.

McCorkle, S., 2021: Using Convolutional Neural Networks to Classify Blowing Snow from Webcam Imagery in Southeastern Wyoming. University of Wyoming, 66 pp.

Accepted for publication in *Weather and Forecasting*. DOI 10.1175/WAF-D-23-0195.1.

https://www.proquest.com/dissertations-theses/using-convolutional-neural-networks-classify/docview/2572579315/se-2?accountid=14793.

Mewes, J. J., 2012: *Mapping Weather Severity Zones*. Meridian Environmental Technology, Inc., https://www.clearroads.org/download/final-report-15/?tmstv=1703870452

Moisseev, D. N., and V. Chandrasekar, 2007: Examination of the μ–Λ Relation Suggested for Drop Size Distribution Parameters. *Journal of Atmospheric and Oceanic Technology*, **24**, 847–855, https://doi.org/10.1175/JTECH2010.1.

Montpetit, B., 2011: In-situ Measurements for Snow Grain Size and Shape Characterization Using Optical Methods, www.easternsnow.org/s/Montpetitetal.pdf.

National Oceanic and Atmospheric Administration, 1998: *Automated Surface Observing Systems (ASOS) User Guide*. 1st ed. Department of Defense, 74 pp.

Naaim-Bouvet, F., H. Bellot, and M. Naaim, 2010: Back analysis of drifting-snow measurements over an instrumented mountainous site. *Ann. Glaciol.*, **51**, 207–217, https://doi.org/10.3189/172756410791386661.

Niu, G.-Y., and Coauthors, 2011: The Community Noah Land Surface Model with Multiparameterization Options (Noah-MP): 1. Model description and evaluation with local-scale measurements. *J. Geophys. Res.*, **116**, D12109, https://doi-org/10.1029/2010JD015139.

Oil City Staff, 2022: 450 miles of Wyoming Interstates closed early Thursday after winter storm. https://oilcity.news/community/2022/01/06/450-miles-of-wyoming-interstates-closed-early-thursday-after-winter-storm/ (Accessed 18 March 2024).

Pomeroy, J. W., and D. H. Male, 1988: Optical Properties of Blowing Snow. *J. Glaciol.*, **34**, 3–10, https://doi.org/10.1017/S0022143000008996.

——, and D. M. Gray, 1990: Saltation of snow. *Water Resour. Res.*, **26**, 1583–1594, https://doi.org/10.1029/WR026i007p01583.

——, and D. H. Male, 1992: Steady-state suspension of snow. *Journal of Hydrology*, **136**, 275–301, https://doi.org/10.1016/0022-1694(92)90015-N.

——, D. M. Gray, and P. G. Landine, 1993: The Prairie Blowing Snow Model: characteristics, validation, operation. *Journal of Hydrology*, **144**, 165–192, https://doi.org/10.1016/0022-1694(93)90171-5.

Accepted for publication in *Weather and Forecasting*. DOI 10.1175/WAF-D-23-0195.1.

Purves, R. S., J. S. Barton, W. A. Mackaness, and D. E. Sugden, 1998: The development of a rule-based spatial model of wind transport and deposition of snow. *Ann. Glaciol.*, **26**, 197–202, https://doi.org/10.3189/1998AoG26-1-197-202.

Rapid City, SD WFO, 2023a: April 3-5, 2023 Winter Storm and Blizzard. https://www.weather.gov/unr/2023-04-03_05 (Accessed May 22, 2023).

Rapid City, SD WFO, 2023b: December 25-26, 2023 After Christmas Blizzard. https://www.weather.gov/unr/2023-12-25_26. (Accessed March 18, 2024).

Rossi, A., 2023: Cowboy State Daily. Wyoming Highways A Gallery Of Black Ice, Blowing Snow And Pileups. https://cowboystatedaily.com/2023/11/24/wyoming-highways-a-gallery-of-black-ice-blowing-snow-and-pileups/ (Accessed March 18, 2024).

Saha, P., M. Ahmed, and R. Young, 2015: Safety Effectiveness of Variable Speed Limit Systems in Adverse Weather Conditions on Challenging Roadway Geometry. Transportation Research Record 2521, p 45-53. https://doi.org/10.3141/2521-05.

Saheb, D., M. Koussa, and S. Hadji, 2014: Technical and Economic Study of a Stand-Alone Wind Energy System for Remote Rural Area Electrification in Algeria. *REPQJ*, 638–643, https://doi.org/10.24084/repqj12.439.

Schmidt, R., 1981: Estimates of threshold windspeed from particle sizes in blowing snow. *Cold Regions Science and Technology*, 4(3), 187–193.

Semmens, K., R. Hogan Carr, B. Montz, and K. Maxfield, 2023: What Impact? Communicating Severity Forecast Information through the Winter Storm Severity Index. *Wea. Climate Soc.*, **15**, 747–758. https://doi.org/10.1175/WCAS-D-23-0023.1

Smirnova, T. G., J. M. Brown, S. G. Benjamin, and D. Kim, 2000: Parameterization of cold-season processes in the MAPS land-surface scheme. *J. Geophys. Res.*, **105**, 4077–4086, https://doi.org/10.1029/1999JD901047.

Smirnova, T. G., J. M. Brown, S. G. Benjamin, and J. S. Kenyon, 2016: Modifications to the Rapid Update Cycle Land Surface Model (RUC LSM) Available in the Weather Research and Forecasting (WRF) Model. *Mon. Wea. Rev.*, **144**, 1851–1865, https://doi.org/10.1175/MWR-D-15-0198.1.

Stoelinga, M. T., and T. T. Warner, 1999: Nonhydrostatic, Mesobeta-Scale Model Simulations of Cloud Ceiling and Visibility for an East Coast Winter Precipitation Event. *J. Appl. Meteor.*, **38**, 385–404, https://doi.org/10.1175/1520-0450(1999)038<0385:NMSMSO>2.0.CO;2.

Accepted for publication in *Weather and Forecasting.* DOI 10.1175/WAF-D-23-0195.1.

Ulbrich, C. W., 1985: The Effects of Drop Size Distribution Truncation on Rainfall Integral Parameters and Empirical Relations. *J. Climate Appl. Meteor.*, **24**, 580–590, https://doi.org/10.1175/1520-0450(1985)024<0580:TEODSD>2.0.CO;2.

United States Department of Transportation, 2018: Large Truck and Bus Crash Facts https://www.fmcsa.dot.gov/safety/data-and-statistics/large-truck-and-bus-crash-facts.

Vionnet, V., E. Brun, S. Morin, A. Boone, S. Faroux, P. Le Moigne, E. Martin, and J.-M. Willemet, 2012: The detailed snowpack scheme Crocus and its implementation in SURFEX v7.2. *Geosci. Model Dev.*, **5**, 773–791, https://doi.org/10.5194/gmd-5-773-2012.

——, G. Guyomarc'h, F. Naaim Bouvet, E. Martin, Y. Durand, H. Bellot, C. Bel, and P. Puglièse, 2013: Occurrence of blowing snow events at an alpine site over a 10-year period: Observations and modelling. *Advances in Water Resources*, **55**, 53–63, https://doi.org/10.1016/j.advwatres.2012.05.004.

——, E. Martin, V. Masson, G. Guyomarc'h, F. Naaim-Bouvet, A. Prokop, Y. Durand, and C. Lac, 2014: Simulation of wind-induced snow transport and sublimation in alpine terrain using a fully coupled snowpack/atmosphere model. *The Cryosphere*, **8**, 395–415, https://doi.org/10.5194/tc-8-395-2014.

Xie, Z., Y. Ma, W. Ma, Z. Hu, G. Sun, and Y. Wang, 2023: Analysis of Multiyear Blowing Snow Occurrences in the French Alps. *Journal of Hydrometeorology*, **24**, 3–19, https://doi.org/10.1175/JHM-D-22-0029.1.

Yu, T., V. Chandrasekar, H. Xiao, and S. S. Joshil, 2020: Characteristics of Snow Particle Size Distribution in the PyeongChang Region of South Korea. *Atmosphere*, 11, 1093, https://doi.org/10.3390/atmos11101093.

Accepted for publication in *Weather and Forecasting*. DOI 10.1175/WAF-D-23-0195.1.